The Observed On-orbit Background of the ACIS Instrument on the Chandra X-ray Observatory

Paul P. Plucinsky and Shanil N. Virani

Harvard-Smithsonian Center for Astrophysics, Cambridge, MA 02138

ABSTRACT

We have analyzed data acquired during the Orbital Activation and Checkout (OAC) and Guest Observer (GO) phases of the Chandra X-ray Observatory (CXO) mission in order to characterize the background of the *Advanced CCD Imaging Spectrometer* (ACIS) instrument produced by energetic particles. The ACIS instrument contains 8 Front-Illuminated (FI) CCDs and 2 Back-Illuminated (BI) CCDs. The FI and BI CCDs exhibit dramatically different responses to enhancements in the particle flux. The FI CCDs show relatively little increase in the overall count rate, typical increases are $1-5$ cts s^{-1} above the quiescent level; the BI CCDs can show large excursions to as high as 100 cts s^{-1} above the quiescent level. The durations of these intervals of enhanced background are also highly variable ranging from 500 s to 10^4 s. These periods of enhanced background are sometimes but not always associated with increased particle flux when Chandra is near the radiation belts. We see evidence for a weak correlation with the low-energy electron channel of the *Electron, Proton, Helium Instrument* particle detector (EPHIN) instrument on-board Chandra. We present some of the most extreme examples of these background enhancements identified to this point in the mission.

The spatial distribution of these enhanced background events is more intense in the middle of the detectors and fainter towards the top and bottom, inconsistent with what one would expect for the vignetting pattern of the telescope and more consistent with an isotropic illumination. The spectral distribution is a continuum across the entire bandpass from 0.3 to 10.0 keV and can not be characterized by a simple power-law plus constant model. The two BI CCDs on Chandra respond similarly to these enhanced background rates, offering the possibility of using data from the off-axis BI CCD to understand the background of the on-axis BI CCD. The traditional techniques of distinguishing background events from x-ray events are ineffective in excluding these background events. Therefore, we suggest that observers might want to consider more aggressive on-board event filtering to reduce the contribution of these background events to the finite ACIS telemetry limit.

Keywords: Chandra, space missions, CCDs, radiation environment, radiation belts, radiation models, radiation damage, magnetosphere

1. INTRODUCTION

The Chandra X-ray Observatory (CXO) is the third of NASA's great observatories in space. CXO was launched just past midnight on July 23, 1999 aboard the space shuttle *Columbia* on the STS-93 mission. CXO was placed into a higher orbit by an Inertial Upper Stage (IUS) booster and then used its own propulsion system to achieve a final orbit with a perigee 10,000 km, an apogee of 140,000 km, an inclination of 28.5° and a period of $\sim$ 64 hr.

The CXO carries two focal plane science instruments: the *Advanced CCD Imaging Spectrometer* (ACIS) and the *High Resolution Camera* (HRC). The Observatory also possesses two objective transmission gratings: a *Low Energy Transmission Grating* (LETG) that is to be primarily used with the HRC, and the *High Energy Transmission Grating* (HETG) that is to be primarily used with the ACIS. In addition to these instruments, Chandra also carries a radiation monitor – the *Electron, Proton, Helium Instrument* (EPHIN) particle detector. This paper will discuss data from the ACIS and EPHIN instruments.

ACIS was developed by a team from the Massachusetts Institute of Technology[1] and the Pennsylvania State University[2] and is the primary scientific instrument aboard CXO, currently conducting $\sim$ 75% of the observations. It contains two arrays of CCDs, one optimized for imaging and the other for spectroscopy as the readout detector for the HETG. The ACIS imaging array contains 4 Front-Illuminated (FI) CCDs configured in a 2×2 array and the spectroscopy array contains 2 Back-Illuminated (BI) CCDs and 4 FI CCDs configured in a 1×6 array.

Further author information: (Send correspondence to PPP) E-mail: pplucinsky@cfa.harvard.edu

EPHIN was developed by the University of Kiel[3,4] and serves as the radiation monitor for CXO. EPHIN is nearly identical to the instrument flown on the Solar and Heliospheric Observatory (SOHO). EPHIN provides count rates for electrons in 4 bandpasses spanning the energy range from 250 keV to 10 MeV and for protons and He isotopes in 4 bandpasses spanning the range 4 MeV/n to 53 MeV/n. In this paper, we will utilize the lowest energy electron channel, called E150, which is sensitive to electrons with energies between 250 and 700 keV.

2. CORRELATION OF ACIS ENHANCED BACKGROUND PERIODS WITH EPHIN COUNT RATES

2.1. ACIS Observations and Configurations

Essentially as soon as the outer cover of the CXO satellite was opened and celestial observations were begun, it was noticed that the background rate observed by ACIS was highly variable. It was natural to explore the possibility that these periods of enhanced background in ACIS were correlated with increases in the EPHIN count rates. We have examined numerous datasets searching for such a correlation. We have selected a few examples for this paper which represent some of the most extreme cases of enhanced background in order to optimize our search for a correlation. Table 1 lists the observation ID numbers, start and stop times, event rejection criteria, and the focal plane temperature.

Table 1. Observations Used in this Analysis

OBSID	Start (GMT)	Stop (GMT)	CCDs On	Event Rejection	FP Temp (C)
1057	228:17:00	228:17:42	I2,I3,S1-S4	reject g7	-99.5
1058	228:17:57	228:18:28	I2,I3,S1-S4	reject g7	-99.5
1059	228:18:43	228:19:15	I2,I3,S1-S4	reject g7	-99.5
1060	228:19:30	228:20:01	I2,I3,S1-S4	reject g7	-99.5
1061	228:20:16	228:20:47	I2,I3,S1-S4	reject g7	-99.5
1062	228:21:02	228:21:34	I2,I3,S1-S4	reject g7	-99.5
1266	228:22:58	229:01:56	I2,I3,S1-S4	reject g7	-99.4
303	286:05:58	286:09:46	I0-I3,S2,S3	reject b24,66,107,214,255 amp > 3750 ADUs	-109.2
965	287:15:49	287:20:07	I1,I3,S2-S5	reject b24,66,107,214,255 amp > 3750 ADUs	-109.0
804	008:01:01 (Y2000)	008:13:14 (Y2000)	I3,S1-S4	reject b24,66,107,214,255 amp > 3750 ADUs	-109.1

It is important to note that the ACIS instrument performs event selection and screening on-board and the parameters used in this selection and screening varied over the course of these observations. Most importantly, ACIS can reject events on board based on their morphology (each event is assigned a code to describe how the charge splits in a 3×3 pixel event island) and their total amplitude. The on-board rejection criteria were changed between OBSIDs 1266 and 303. The early observations rejected ASCA g7 events and used no event amplitude cutoff; the latter observations rejected flight grades b24,66,107,214, and 255 and used an amplitude cutoff of 3750 ADUs ($\sim$ 15 keV). Fortunately, these parameters allowed the different datasets to be analyzed in a consistent way on the ground by applying the most common selection criteria for astrophysical applications of ASCA g02346 and $0.3 < E < 10.0$ keV. We will specify throughout the paper when these selection criteria are used and when the "total event" rate, which is everything the CCD and electronics can record and telemeter, is used. Additionally, the ACIS focal plane temperature was changed once over the course of these observations from ~ -100 C to ~ -110 C. This is significant because the number and intensity of hot pixels on the BI CCDs is a strong function of temperature. In order to allow a consistent comparison between the data at the two different temperatures, the list of hot pixels appropriate for the -100 C data were excluded from all the datasets.

2.2. The Sample Observations

We summarize four cases of extremely high background below during which CXO's position with respect to the radiation belts was distinct. The analysis of these observations spurred a re-examination of the predicted entry and

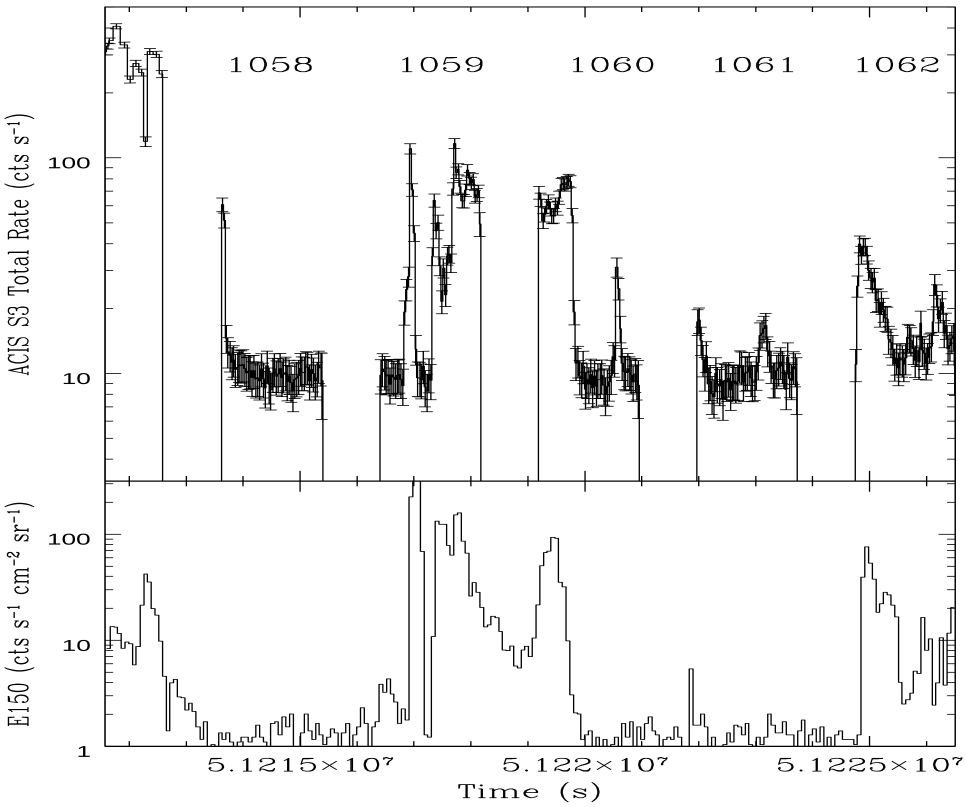

Figure 1. OBSIDs 1057-1062: The ACIS S3 total rate averaged over 32.4s intervals and the EPHIN E150 rate in the nominal integration time of 65.6 s. The units of time are seconds since 1999 Jan 1. The first group of data at the left of the plot are from OBSID 1057.

exit times from the radiation belts provided by the CXO mission scheduling SW. This issue is discussed in detail in a companion paper[5] in these proceedings. We include one final case in which the background was more typical.

CASE I, Exiting the Belts, OBSIDs 1057-1063: The CXO outer cover was opened at GMT1999:224:18:00. The following orbit was used to test the pointing and maneuvering capabilities of the spacecraft. The satellite then began conducting normal check out activities such as acquiring data necessary to determine the best focus position. OBSIDs 1057-1062 were focus measurements which began at GMT1999:228:17:00 just after a perigee passage at GMT1999:228:11:53. Thus, CXO was just emerging from the radiation belts when these observations commenced. Figure 1 shows the total ACIS S3 (the BI CCD at the focal position in the spectroscopy array) count rate and the EPHIN E150 rate for this time period. The ACIS rate has been averaged over 32.4 s intervals to better match the EPHIN integration times of 65.6 s. The quiescent ACIS rate for these observations is $\sim$ 10 cts s^{-1}, while there are large excursions up to $\sim$ 300 cts s^{-1}. OBSID 1057 (the first group of data in the figure) was most likely affected by the edge of the radiation belts. However, OBSIDs 1059 and 1060 are outside of what are typically considered to be the radiation belts. The ACIS rate typically increases when the E150 rate increases and the ACIS rate is constant when the E150 rate is constant. However, note that the relative increase in the ACIS rate compared to the E150 rate is different for the event at the beginning of the plot during OBSID 1057 than it is for the event beginning at $t = 5.1217 \times 10^7$ s and lasting until $t = 5.1221 \times 10^7$ s. So clearly, the E150 channel is not a complete indicator of all the particles which are capable of producing enhanced background in ACIS. We explored the correlation with the higher energy electron channels and the lowest-energy proton channel but found that the ACIS rate appeared to

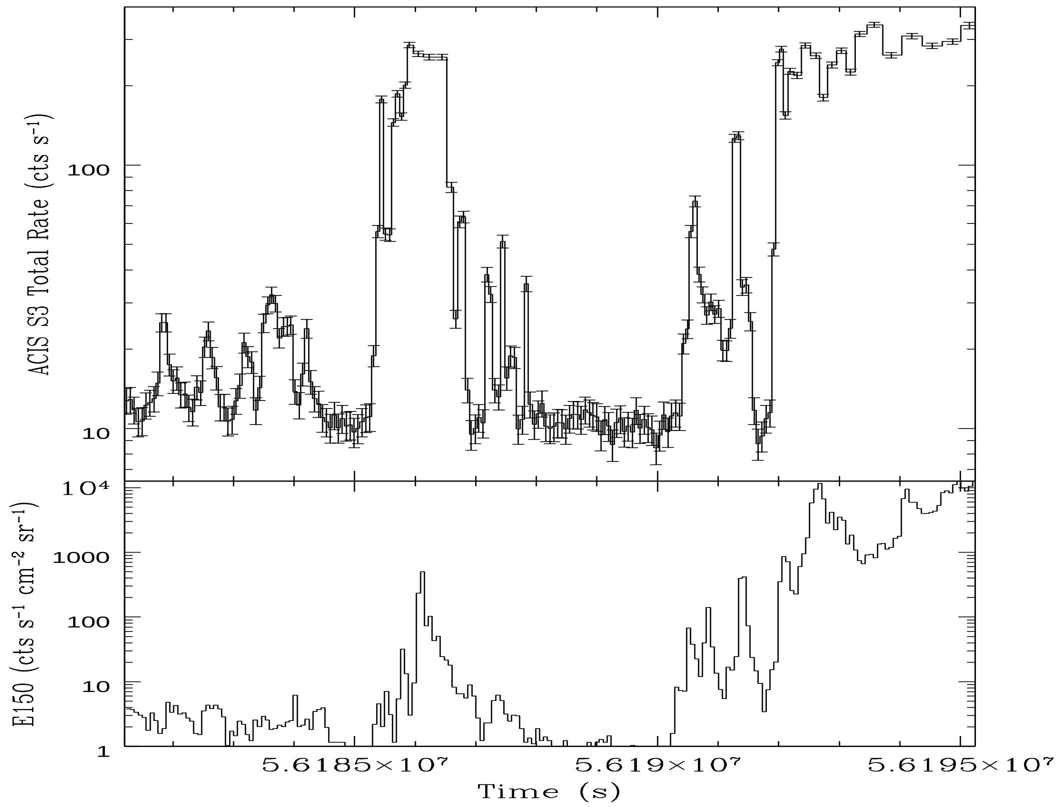

Figure 2. OBSID 303: The ACIS S3 total rate averaged over 64.8s intervals and the EPHIN E150 rate. The units of time are seconds since 1999 Jan 1.

correlate best with the E150 channel.

CASE II, Entering the Belts, OBSID 303: OBSID 303 presents an analogous situation to CASE I above except that CXO was entering the radiation belts. The ACIS and EPHIN data from this observation are plotted in Figure 2. Significant fluctuations in the ACIS count rate are seen throughout almost the entire time interval with large events at $t = 5.6186 \times 10^7$ s and the end of the observation starting at $t = 5.6191 \times 10^7$ s. Presumably the enhanced rates at the end of the observation are due to the outer edges of the belts but the earlier event is still quite far from the belts. The large excursions above 100 cts s^{-1} caused telemetry saturation in ACIS. These two large events were also correlated with the higher-energy electron channels and the low-energy proton channel of EPHIN.

CASE III, 11 hr after perigee, OBSID 1266: OBSID 1266 was performed in the same orbit as OBSIDs 1057-1062 although at a later point in the orbit. The lightcurve of this observation is plotted in Figure 3. Once again almost the entire observation is affected by an enhanced background rate accompanied by significant fluctuations in the E150 rate. However, the ACIS rate did not increase as much as in the previous observations, always staying below 100 cts s^{-1}. CXO was at 80,000 km and ascending during this observation.

CASE IV, near apogee, during a Coronal Mass Ejection, OBSID 965: OBSID 965 was performed near apogee while CXO and its environment were subjected to the aftermath of a Coronal Mass Ejection (CME) event on the Sun. EPHIN exhibited a prolonged period of enhanced count rates in most of its channels. The ACIS and EPHIN data are plotted in Figure 4. The ACIS rate is rather quiet during this interval (except for a few small enhancements) while the E150 rate is increasing steadily throughout the observation. The spike in the ACIS rate at $t = 5.6315 \times 10^7$ s was an instrumental effect and had nothing to do with the background rate.

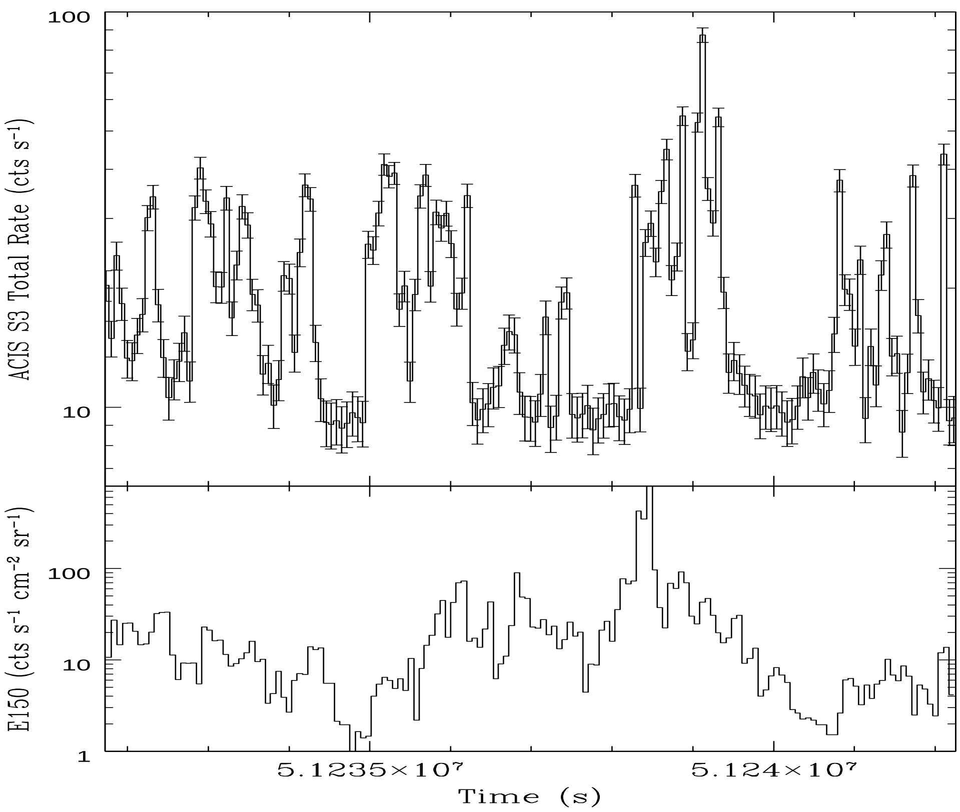

Figure 3. OBSID 1266: The ACIS S3 total rate averaged over 64.8s intervals and the EPHIN E150 rate. The units of time are seconds since 1999 Jan 1.

CASE V, near apogee, low solar activity, OBSID 804: We have presented the most pathological cases of enhanced background identified so far in the CXO mission. The cases presented so far are the exception and not the rule. As a counter example we present OBSID 804 which was acquired near apogee while the solar activity was low. The ACIS and EPHIN rates, shown in Figure 5 are low and constant throughout the majority of the observation. The only exception is a small time interval near the end of the observation at $t = 6.372 \times 10^7$ s during which the ACIS S3 rate increases just slightly above 10 cts s^{-1}.

2.3. Detailed Correlation between ACIS and EPHIN

All five of the preceding cases indicate that there is a general correlation between the background rate as seen by ACIS and the EPHIN E150 channel. This is no surprise, the CCDs are sensitive to electrons in this energy range. One might hope to use the E150 channel to model and estimate the ACIS background rate. Unfortunately, the detailed correlation between the two rates is not good. We generated a simple scatter plot of the ACIS rate and the E150 rate. At this point we have restricted our event selection to events with grades of ASCA g02346 and energies of $0.3<E<10.0$ keV since those are the events observers would be most interested in modeling the background. Figure 6 shows the poor correlation between the two rates. It is clear that when EPHIN shows enhanced rates, ACIS will also exhibit enhanced rates at roughly the same time. But Figure 6 shows that the exact times of the increases in the two detectors do not match well. Certainly, the ACIS rate cannot be described by a simple function of the E150 rate. Perhaps this indicates the process by which the electrons which EPHIN is sensitive to make their way to the focal plane is rather complex. If one believes that the low energy particles are propagating down the optical path of the

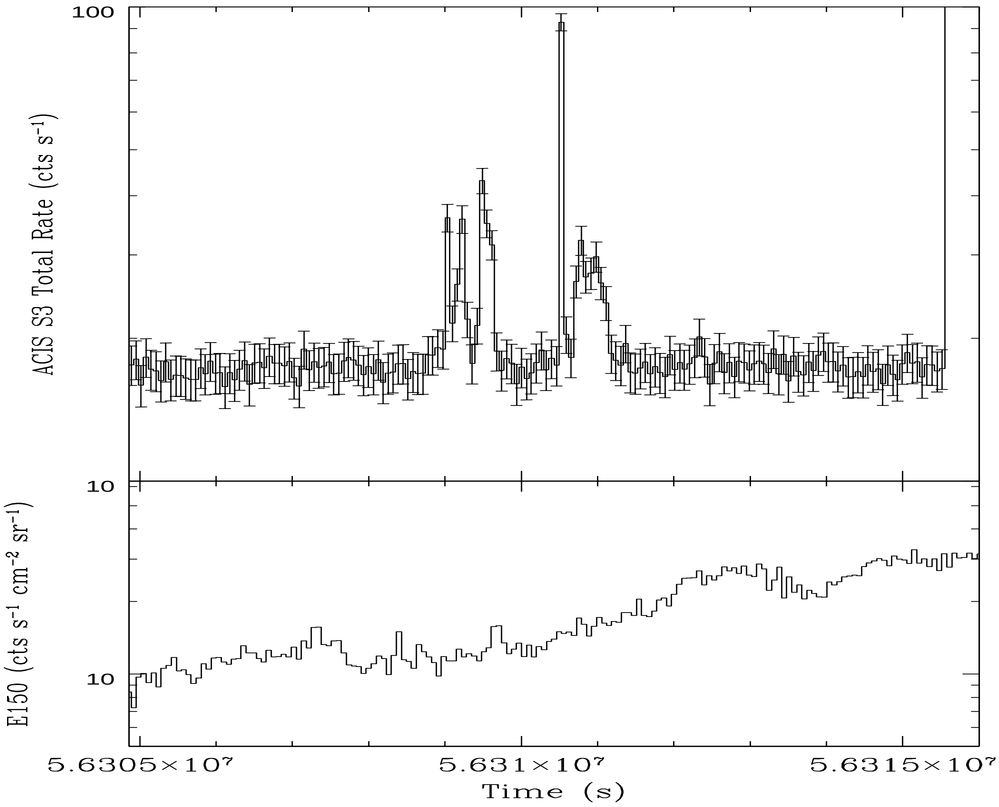

Figure 4. OBSID 965: The ACIS S3 total rate averaged over 64.8s intervals and the EPHIN E150 rate. The units of time are seconds since 1999 Jan 1. The spike in the ACIS rate at $t = 5.6315 \times 10^7$ s was an instrumental effect.

telescope to the focal plane, one could easily imagine that spacecraft orientation would be an important parameter in determining the possibility that particles which EPHIN is detecting can actually make it to the focal plane.

3. DETAILED ACIS CHARACTERIZATION

3.1. BI CCD vs FI CCD

Up until this point we have shown lightcurves of BI CCD data only. The FI CCDs do exhibit enhanced background, albeit not as dramatic as the BI CCDs. For example, we plot in Figure 7 the lightcurve of the g02346, 0.3<E<10.0 keV events for the S2 (FI) CCD and the S3 CCD. The two CCDs show enhanced background during the same time intervals, but the signal is smaller in the FI CCD. This suggests that low-energy particles are mostly responsible for the enhanced background, since the particles must travel through the gate structure of the FI CCDs in order to produce a detectable signal.

3.2. BI CCD vs BI CCD

Since there are two BI CCDs in ACIS, one on-axis (S3) and the other off-axis (S1), one could hope to use the off-axis BI CCD to understand the background of the S3 CCD where presumably the source of astrophysical interest lies. Comparing the lightcurves of the two BI CCDs for OBSIDs 1057-1062, it is clear the two CCDs are responding in a similar manner to the background enhancements. We plotted the S1 rate versus the S3 rate to examine the correlation. The data are plotted in Figure 8 and show that the correlation is excellent. The best-fit line with a

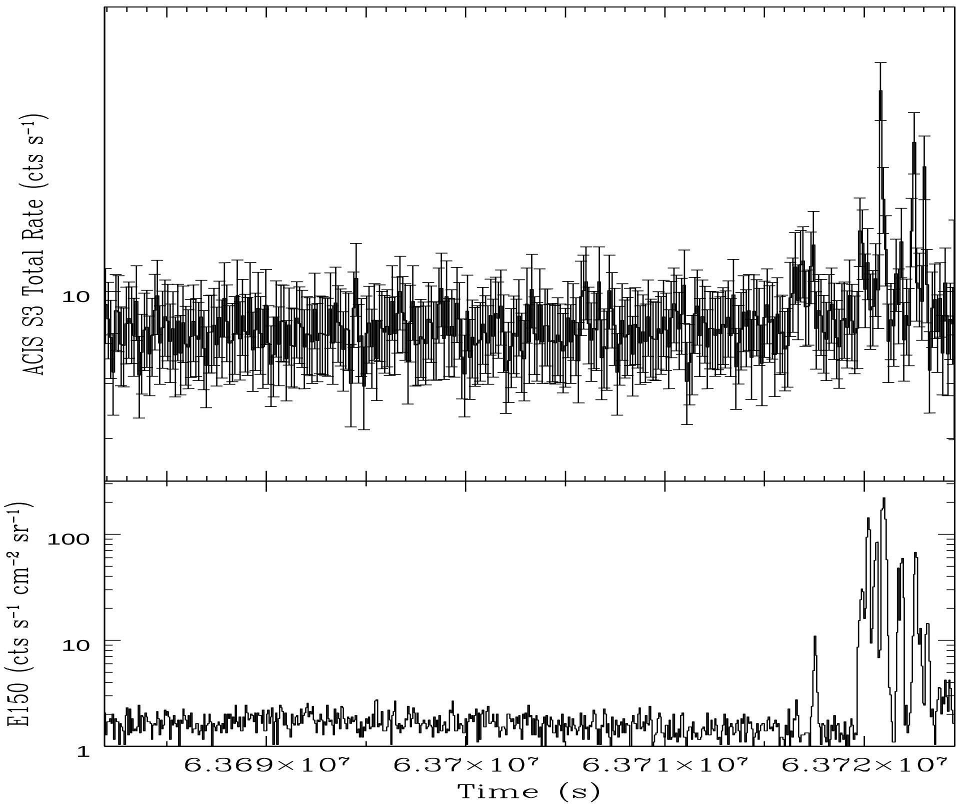

Figure 5. OBSID 804: The ACIS S3 total rate averaged over 64.8s intervals and the EPHIN E150 rate. The units of time are seconds since 1999 Jan 1.

reduced χ^2 of 2.34 is also plotted on the graph. The intercept is non-zero and positive. This is most likely due to some "warm" pixels on the S1 CCD which have not be excluded. These data were acquired with the focal plane at ~ -100 C and the S1 CCD shows substantially more hot pixels than the S3 CCD. We have excluded the pixels which produced an event in 50% or more of the frames, but it is probably the lower frequency warm pixels which are causing the offset. The slope of 0.847 indicates that the count rate on S3 is almost always higher; this would be consistent with a higher particle flux on-axis.

3.3. Spatial Distribution

We examined the spatial distribution of the events associated with the periods of enhanced background by making an image in detector coordinates when the background rate was high and an image when the background rate was low and subtracting the two. We selected the time periods from the second half of OBSID 1059 and the first half of OBSID 1060 as "high background" periods and the period in OBSID 1058 when the count rate was flat (which is most of the observation) as a "low background" period. For this analysis we selected events with grades of *ASCA* g02346 and amplitudes between 0.3<E<10.0 keV. These datasets have the advantage that CXO was pointed at the same region of the sky so that differences between the images can not be due to celestial sources (excluding time variable sources of course). We corrected the two datasets for the different exposure times and subtracted the images. The resulting image is displayed in Figure 9. The greyscale has been inverted so that darker colors indicate higher count rates. The data have been binned into 32×32 pixel regions. The three white pixels towards the left of the image which form an "L" shape contain the source which was the target of these observations. Those pixels have been set to zero. There appears to be a slight enhancement in the middle of the detector and a deficit at the top

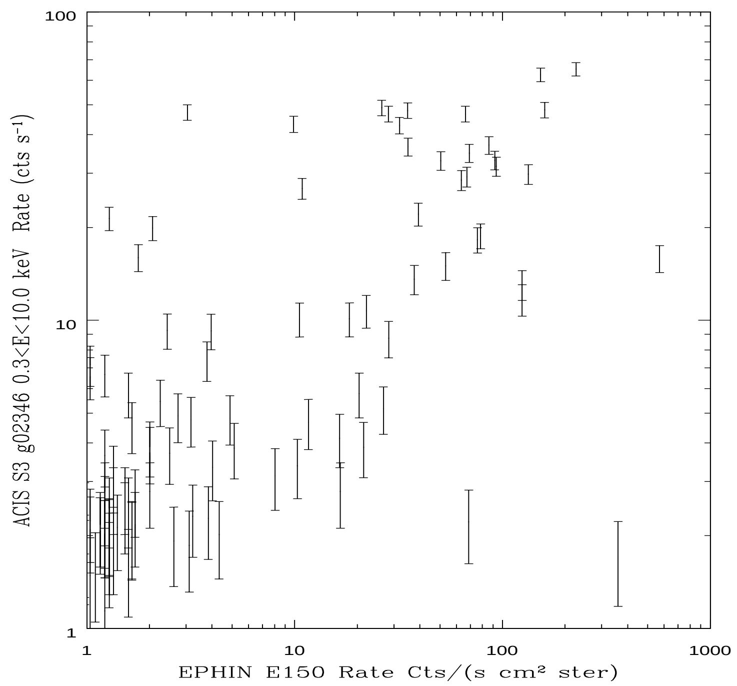

Figure 6. The ACIS S3 g02346 $0.3<E<10.0$ keV rate plotted versus the E150 rate. The detailed correlation is not as good as one might have expected from Figure 1

and bottom. Choosing two pixels at random $p_1(x = 13, y = 17)$ and $p_2(x = 3, y = 31)$, we find the count rates and errors to be $r_1 = 3.83 \pm 0.21 \times 10^{-2}$cts s^{-1} and $r_2 = 2.54 \pm 0.47 \times 10^{-2}$cts s^{-1}. Therefore, the intensity difference is significant at the 2.5σ level. It is interesting that the pattern shows an enhancement running along the middle of the CCD, this is not one would expect if the particles were scattering off of the mirror toward the focal plane.

Table 2. Effectiveness of Event Filtering on Telemetry Saturation

Event Selection	# of Events	Rate (cts s^{-1})
S3 (BI CCD)	(11305.6s)	
g02346, $0.3<E<10.0$ keV	336210	29.74
g02346	466780	41.29
$0.0<E<8.0$ keV	334143	29.56
$0.0<E<10.0$ keV	400280	35.40
b24,66,107,214,255, $E<15$ keV	608458	53.82
S2 (FI CCD)	(11948.8s)	
g02346, $0.3<E<10.0$	60146	5.03
g02346	116315	9.73
$0.0<E<8.0$	140960	11.80
$0.0<E<10.0$	157554	13.19
b24,66,107,214,255, E¡15 keV	220023	18.41

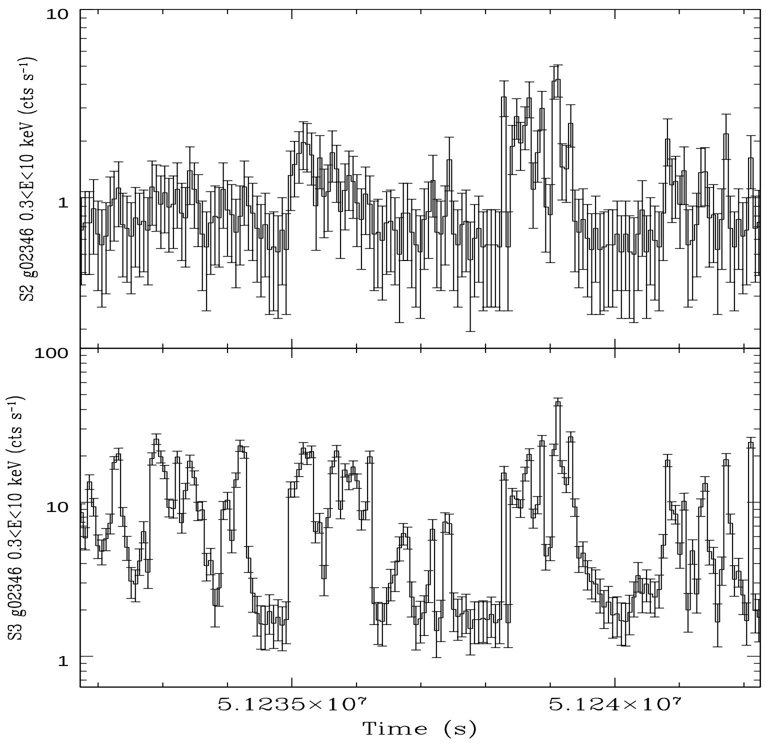

Figure 7. The ACIS g02346 0.3<E<10.0 keV rate of the S2 and S3 CCDs for OBSID 1266. Note how the two detectors show enhanced count rates in the same time intervals but the enhancement is much smaller in the FI CCD.

3.4. Spectral Distribution

We used the same datasets in § 3.3 above to examine the spectral distribution of the events associated with high background. We once again extracted spectra from the periods of "high background" in OBSIDs 1059 and 1060 and from the period of "low background" in OBSID 1058. We then subtracted the two spectra in order to get a spectrum of the excess events. The result is plotted in Figure 10. The spectra were generated from *ASCA* g02346 events and were extracted from the second quadrant of the S3 CCD alone. Notice that the excess counts extend across the entire bandpass from 0.3 to 10.0 keV, which is what is typically used for astrophysical observations. The spectrum cannot be well fitted with a simple power-law plus a constant model. We intend to explore more complex models in the future. It is unfortunate that the excess counts extend across the entire bandpass, but it will be simpler to subtract a smooth background spectrum for most astrophysical applications. The variability of this background spectrum from observation to observations still needs to be explored.

3.5. Impact of High Background Events on Observations

As the previous sections have shown, the events associated with the enhanced background times reproduce many of the characteristics of valid X-ray events in the ACIS CCDs. Typically one attempts to distinguish background events from X-ray events of interest by their different grade or pulse-height distributions. Neither of these techniques will be successful with the background events we have examined here. We recommend that CXO guest observers always generate a lightcurve from their observation and examine it for enhancements. If the time intervals represent a small fraction of the observation, it may be best to exclude those times. If the fraction of time is non-negligible and the source is a point source, the GOs should consider subtracting this background in the same way they subtract the quiescent background. If the object is a large extended object, the GOs should consider using data from another

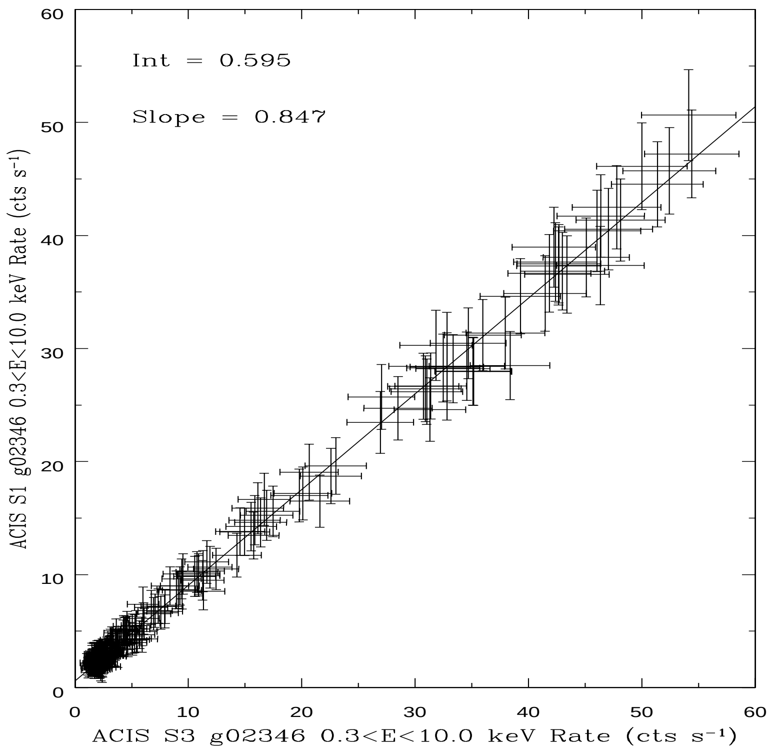

Figure 8. The ACIS g02346 0.3<E<10.0 keV rate for the two BI CCDs (S1 & S3) plotted against each other. The correlation is excellent with a best-fit line giving an intercept of 0.595, slope of 0.847 and a reduced χ^2 of 2.34

CCD as the background data. For example, the S1 CCD should be tried as the background source for the S3 CCD and one FI CCD could be used as the background source for another FI CCD.

GOs should also be aware of the impact of high background times on telemetry saturation. Most of the observations presented in this paper saturated the telemetry stream significantly and therefore data was lost. Since the BI CCDs are significantly more susceptible than the FI CCDs to these background enhancements, observations which utilize one or both BI CCDs should be carefully planned. The GO may wish to utilize more aggressive on-board filtering to throttle back the event rate. For example, Table 2 shows the effectiveness of various combinations of event filters on the OBSID 303 data. Simply lowering the upper event amplitude cutoff from 15 keV to 10 keV or even 8 keV may provide enough reduction in the overall count rate to prevent telemetry saturation.

4. FUTURE WORK

We intend to continue to examine the correlation between the ACIS count rates and EPHIN count rates, although a preliminary examination indicates that a correlation good enough to allow modeling of the ACIS background may not exist. We also hope to explore a correlation with the low-energy electron and proton channels of the *Advanced Composition Explorer* (ACE) satellite which CXO is currently using as an early warning of particle storms emanating from the Sun. The detailed CCD characterization needs to be expanded to datasets which provide higher statistical precision. The spatial distribution of the excess events hinted at in this paper needs to be confirmed by observations with a larger number of counts and with the focal point of the telescope on the imaging and spectroscopy arrays. The spectral distribution of the the excess events in the BI and FI CCDs needs to be determined to better precision and the differences between the two types of detectors needs to be understood. Presumably, the spectrum observed by the ACIS CCDs will change as the spectrum of the incident particles changes. This would be the most likely

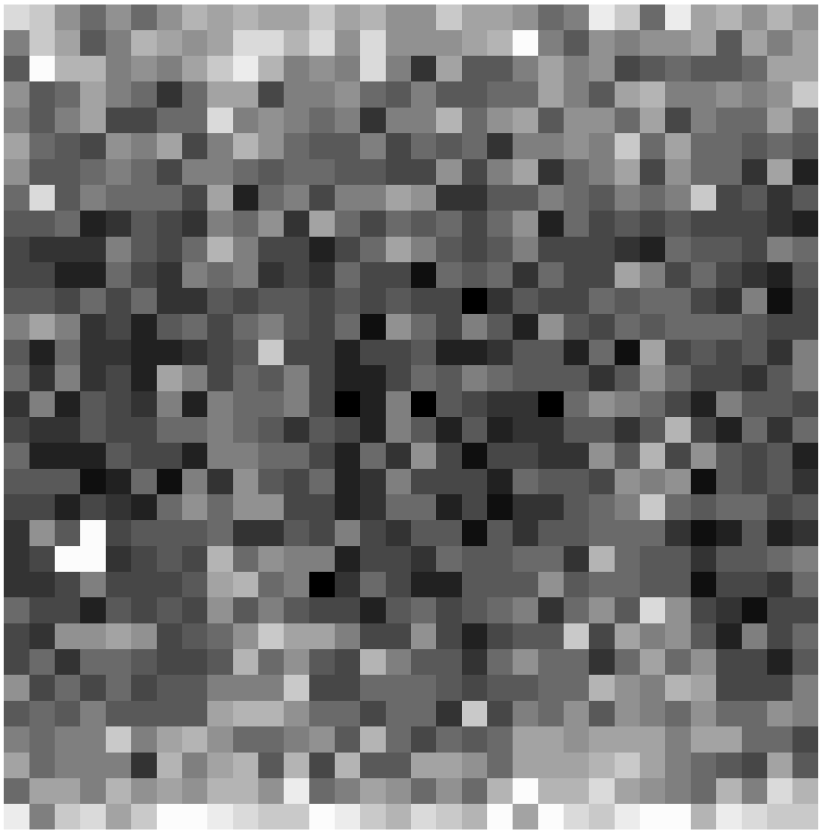

Figure 9. The difference of the observed spatial distribution of counts between the high background periods of OBSIDs 1059 and 1069 and the low background period of OBSID 1058. The greyscale has been inverted so that darker colors indicate a higher count rate. Events were selected with grades equal to g02346 and with amplitudes 0.3<E<10.0 keV. The middle row of the image has an average rate of 3.71×10^{-2}cts s^{-1} in a 32×32 pixel region and the row second from the top has an average rate of 2.67×10^{-2}cts s^{-1}.

explanation of the cases in which the BI CCDs exhibit an enhanced count rate but the FI CCDs show little or no enhancement; the spectrum of the incident particles may be too soft to produce a signal in the FI CCDs. This suggestion needs to be confirmed by observations with higher quality spectra than OBSIDs 1057-1062. Finally, new techniques must be explored for identifying, excluding, and/or modeling the background counts in order to recover a larger fraction of the useful observation time.

ACKNOWLEDGMENTS

We thank our colleagues, Mark Bautz, Bev Lamarr, Peter Ford, and Fred Baganoff, for many useful ideas over the course of this analysis. We thank Maxim Markevitch for the comparison of our results to his own analysis. We also thank R. Muller-Mellin for helping us to understand how EPHIN works.

REFERENCES

1. M. Bautz, M. Pivovaroff, F. Baganoff, T. Isobe, S. Jones, S. Kissel, B. Lamarr, H. Manning, G. Prigozhin, G. Ricker, J. Nousek, C. Grant, K. Nishikida, F. Scholze, R. Thornagel, and G. Ulm, "X-ray ccd calibration for the axaf ccd imaging spectrometer," in *X-Ray Optics, Instruments, and Missions*, R. B. Hoover and A. B. W. II, eds., *Proc. SPIE* **3444**, p. 210, 1998.

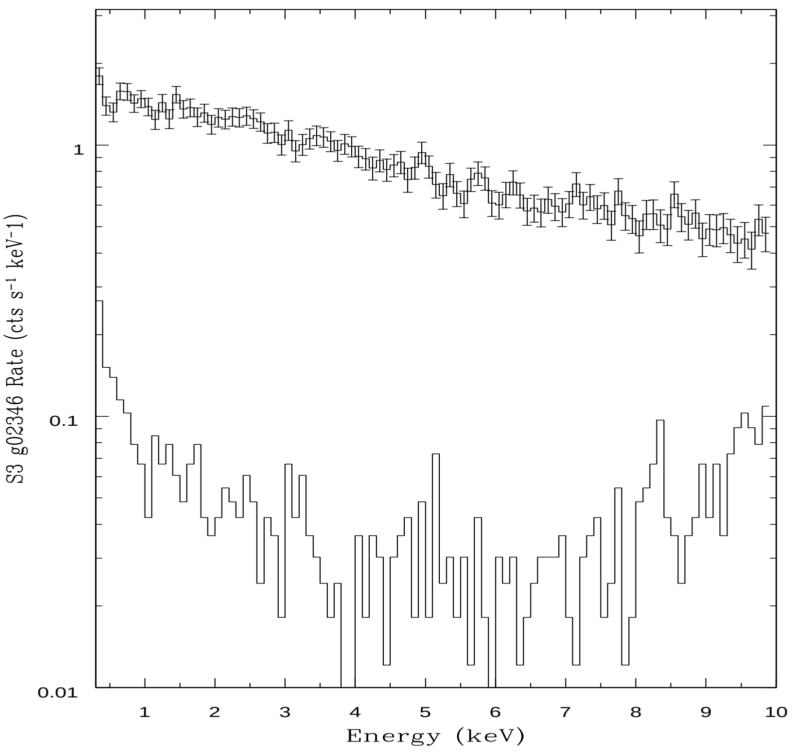

Figure 10. The spectrum of the excess background counts and the "quiescent" spectrum. Only g02346 events from the second quadrant of the S3 CCD have been included in this spectrum. The upper histogram with errors bars is the spectrum of the enhanced background events after subtracting the quiescent spectrum. The lower histogram without errors bars is the spectrum from the low-background period of OBSID 1058.

2. G. Garmire, G. Ricker, M. Bautz, B. Burke, D. Burrows, S. Collins, J. Doty, K. Gendreau, D. Lumb, and J. Nousek, "The axaf ccd imaging spectrometer," in *American Institute of Aeronautics and Astronautics Conference*, p. 8, 1992.
3. R. Mueller-Mellin, H. Kunow, V. Fleissner, E. Pehlke, E. Rode, N. R. C. Scharmberg, H. Sierks, P. Rusznyak, S. McKenna-Lawlor, I. Elendt, J. Sequeiros, D. Meziat, S. Sanchez, J. Medina, L. del Peral, M. Witte, R. Marsden, and J. Henrion, "Costep - comprehensive suprathermal and energetic particle analyzer," *Solar Physics* **162**, pp. 483–504, 1995.
4. H. Sierks, "Kosmiche teilchen im sonnensystem - messung geladener teilchen mit dem kieler instrument ephin an bord soho-raumsonde," *PhD. thesis* , 1997.
5. S. N. Virani, R. Mueller-Mellin, P. Plucinsky, , and Y. Butt, "The chandra x-ray observatory's radiation environment and the ap-8/ae-8 model," in *X-Ray Optics, Instruments, and Missions*, J. Trumper and B. Aschenbach, eds., *Proc. SPIE* , 2000.